

Inverted-Parabolic and Weak strain dependencies for the Critical Current in Practical <110> and <100> Oriented REBCO Tapes

Kozo Osamura¹⁾, Shutaro Machiya²⁾,
Kentarou Kajiwara³⁾, Takuro Kawasaki⁴⁾, Stefanus Harjo⁵⁾,
Yifei Zhang⁵⁾, Shinji Fujita⁶⁾, Yasuhiro Iijima⁶⁾ and Damian P. Hampshire⁷⁾

¹⁾ Research Institute of Applied Sciences, Kyoto 606-8202, Japan

²⁾ Department of Engineering, Daido University, Nagoya 457-8530, Japan

³⁾ JASRI, 1-1-1 Kouto, Sayo-cho, Hyogo 679-5198 Japan

⁴⁾ J-PARC Center, 2-4 Shirane Shirakata, Tokai-mura, Ibaraki 319-1195 Japan

⁵⁾ SuperPower Inc., 450 Duane Ave., Schenectady, NY 12304, USA

⁶⁾ Advanced Technology Laboratory, Fujikura Ltd., 1440, Mutsuzaki, Sakura-shi, Chiba 285-8550, Japan

⁷⁾ Department of Physics, University of Durham, Durham DH1 3LE, UK

Corresponding author: (kozo_osamura@rias.or.jp)

Abstract

Two of the types of practical REBCO ($\text{REBa}_2\text{Cu}_3\text{O}_{7-d}$, RE = Y and Gd) tapes that have been commercialized, have different twinned structures characterised as <100> (from SuperPower) and <110> orientations (from Fujikura) along the tape axis. In order to elucidate the effect of these different twinned structures on the critical current of these practical REBCO tapes, complementary critical current measurements and synchrotron radiation diffraction measurements were carried out to characterise them. For the <100> oriented tapes, inverted parabolic strain behavior was observed for the uniaxial strain dependence of the critical current. In contrast, the <110> oriented REBCO tape does not give any maximum in the strain dependence of the critical current and shows a weak strain behaviour. The different uniaxial strain dependencies observed for the critical current of the <100> and <110> oriented REBCO tapes were analyzed using a one-dimensional twin model for REBCO material with different fractional lengths of A-domains and B-domains. This model explains the essential features of the different uniaxial strain dependencies observed.

1. Introduction

Despite the huge effort directed at developing practical composite superconductors, there are currently only five different materials that have been comprehensively commercialised [1]. These practical superconducting wires and tapes include multicomponent structures designed to meet optimized engineering requirements. Because the constituent components have different coefficients of thermal expansion (CTE) and different moduli of elasticity (E), it is difficult to determine the local stress and strain exerted on the superconductive component and how it influences the electromagnetic properties under operation [2]. Several analyses of the local stress and strain have been reported in the literature for the commercialized superconductors that are brittle, MgB_2 [3], BSCCO [4, 5], REBCO [6, 7, 8] and Nb_3Sn [9, 10, 11, 12]. The nature and origin of the stress and strain behavior on the electromagnetic properties depends on the details of the architecture of these composite systems, so it is still essential to carry out quantitative studies of these materials in order to get a full understanding and to realize the best available performance under operational stress and strain conditions.

It has been well-established that a maximum in the critical current appears in the strain dependence for practical Nb_3Sn wires [13, 14, 15] at strain values close to zero deviatoric strain [16]. For practical BSCCO-2223 tapes, it is less clear whether there exists a maximum in the reversible region. The maximum in the strain dependence of the critical current that has been observed, very probably has its origin in degradation due to compressive fracture of superconducting filaments [17]. Hence the elastic regime for BSCCO-2223 tapes has a weak strain behavior that is qualitatively quite different to the inverted parabolic behavior of Nb_3Sn .

Ever since REBCO composite tapes were developed for applications, their mechanical and electromagnetic properties have been investigated widely [18, 19]. Two practical REBCO ($REBa_2Cu_3O_{7-d}$, $RE = Y$ and Gd) tapes have been widely commercialized and are characterized as having $\langle 100 \rangle$ and $\langle 110 \rangle$ orientations along the tape axis. Recently we have shown [20] that the $\langle 100 \rangle$ oriented REBCO tapes show an inverted parabolic strain dependence with a clear maximum in critical current, which can be associated with the supercurrent repeatedly passing through A- and B- domains. The focus of the present study is to determine how the strain dependence of the critical current behaves for the $\langle 110 \rangle$ oriented (Fujikura) REBCO tape. In particular we investigate whether the $\langle 110 \rangle$ oriented REBCO tapes give any maximum in the strain dependence of critical current or not. We also compare the results for the $\langle 100 \rangle$ and $\langle 110 \rangle$ oriented REBCO tapes and show that the different strain dependencies can be explained within the context of the one-dimensional twin (or chain) model [20].

Complementary transport and synchrotron studies are reported here on the two different tapes. The strain dependence of critical current over a wide range of uniaxial

external strain has been investigated using two well-established techniques - the free-standing sample holder and the springboard [21]. Furthermore, in order to get direct information about the local strain exerted on the REBCO superconductive layer, a synchrotron diffraction study using SPring-8 [20] has also been completed.

2. Experimental Procedure

Among the tapes provided from the two commercial suppliers, there were two kinds of Superpower tapes investigated - REBCO $\langle 100 \rangle$ with and without Cu layers – as well as the Fujikura REBCO $\langle 110 \rangle$ with a Cu layer. The general specifications of the tapes are listed in Table 1 as well as on the manufacturer's web-pages [22, 23]. In general, the tapes consist of a thin superconducting layer, grown on the substrate via a buffer layer.

The critical current measurements were carried out in open cryostats in liquid nitrogen. The details of the free-standing transport measurements and those made using the springboard have been reported previously [20]. Basically the freestanding sample was held using a gripping jig which was electrically isolated from the universal testing machine (Fig. 1 (a)). The voltage taps were soldered onto the tape, 25 mm apart, outside the Nyilas type strain gauge (SG). The critical current was determined using a criterion of $1 \mu\text{V}/\text{cm}$. For the measurements on the springboard (Fig. 1 (b)), the tape sample was soldered onto the springboard, and a strain gauge was glued onto the tape surface. The voltage taps were soldered onto the tape, 25 mm apart, outside the strain gauge. The springboard enables both compressive and tensile strains to be applied to the tapes by pushing or pulling along the load axis and measuring the changes in strain produced using the strain gauge.

The diffraction experiments were carried out at room temperature at the BL28B2 station of SPring-8 [20]. Just as with the critical current measurements, both a freestanding sample and a sample on a springboard were measured. For the freestanding sample, the Nyilas type strain gauge was placed outside the diffraction point of the incident beam to prevent it from absorbing any of the incident beam. The sample on the springboard was installed in a specially designed load frame. The size of the Cu-Be springboard was 78 mm long, 15 mm wide and 2.5 mm thick. In order to reduce the absorption of the incident beam, a blind hole was incorporated into the spring board. In both cases, the diffraction peaks were measured as a function of uniaxial strain. The diffraction geometry ensured that the scattering vector was parallel to the tape axis. In the present study, the spacing of the (200), (020) and (220) planes of the orthorhombic REBCO phase was employed for local strain measurements because their diffraction intensity was strong enough to ensure sufficient statistical accuracy.

3. Experimental Results

3.1 Mechanical properties at room temperature (RT) and 77 K

Stress (R) – strain (A_a) behavior at RT and 77 K is shown in Fig. 2 for the REBCO <100> without Cu tape. The slope in the small strain region increased linearly. At high strains, beyond the shoulder in the response, the tapes did not fracture as a whole, but plastic deformation was observed accompanied by increasing work hardening of the metallic components. The modulus of elasticity was determined in the linear – small strain region according to the method recommended in the international standard IEC 61788-25 [24], where two types of the modulus of elasticity, E_0 and E_u are considered, the initial slope of the stress – strain curve and the slope for the partially unloaded curve respectively. Usually it is recommended that E_u as well $R_{0.2}$ and $A_{0.2}$ (the stress and strain at the 0.2% proof strength) are recorded as typical values. Table 2 also shows the mechanical properties for all the tapes including the REBCO <100> with Cu and the REBCO <110> with Cu tapes. As expected the modulus of elasticity is lower in the tapes that have a lamination of Cu sheet included.

3.2 Tensile load dependence of critical current – free standing measurements

Previous studies [19, 20] have made clear that the critical current of REBCO tapes decreases over a small range of tensile stress and that the critical current returns reversibly on reducing the stress back to zero. When the tensile stress is increased beyond a characteristic limit, the critical current decreases rapidly due to the brittle fracture of REBCO layer. This behavior was reconfirmed for the present REBCO tapes as follows: The applied strain (A_a) dependence of the normalized critical currents, I_c/I_{c0} and I_{cr}/I_{c0} are plotted in Fig. 3 for REBCO <100> without Cu. The normalized critical current I_c/I_{c0} decreased gradually from the beginning and then decreased rapidly over the strain region larger than about 0.38% strain. Also, the normalized recovered critical current I_{cr}/I_{c0} as shown in Fig. 3 decreased gradually up to about 0.4% and then decreased abruptly. The abrupt decreases are attributed to the brittle fracture of REBCO layer [18]. As shown in Figure 3, the recovered critical current I_{cr} decreased rapidly beyond a certain strain. We have discussed previously that the reversible stress limit is best defined as the stress at $I_{cr}/I_{c0}=0.99$ [19] with the reversible stress and strain limits expressed as R_{99} and A_{a99} , respectively. As listed in Table 3, R_{99} was 871 MPa for REBCO <100> without Cu tape. Similar stress / strain dependence of the normalized critical currents, I_c/I_{c0} and I_{cr}/I_{c0} was measured for the REBCO <100> with Cu tape and the corresponding critical parameters are summarized in Table 3.

Fig.4 shows the normalized critical currents, I_c/I_{c0} and I_{cr}/I_{c0} as a function of applied strain for REBCO <110> with Cu tape. Compared to the data for the <100> tape given in Fig. 3, the change of both normalized critical currents, I_c/I_{c0} and I_{cr}/I_{c0} is far less sensitive to strain and stress in the reversible region. A_{99} was 0.453 %, before decreasing rapidly

due to the brittle fracture of REBCO layer as listed in Table 3. In much of the literature [7, 16, 20], the 95% retained strain (A_{a95}) convention has also been used to provide the reversible strain limit for both REBCO and BSCCO tapes. Therefore, in the present study, A_{a95} and R_{95} have also been evaluated and are also listed in Table 3.

3.3 Uniaxial strain dependence of critical current – springboard measurements

Similar I_c measurements were carried out for all the tapes mounted on the springboard. The results for the REBCO <100> with and without Cu tape are shown in Fig. 5. For the tape without Cu, over the strain region measured (i.e. -0.4% to 0.6%), the normalized recovered critical current I_{cr}/I_{c0} kept almost to unity, which means there was no observable degradation. The normalized critical current I_c/I_{c0} indicated a clear maximum. This convex behavior is not symmetric with respect to the applied strain and the peak of the inverted parabola is located in the tensile strain region. In order to discuss the strain dependence, the following parameters were obtained: $A_{a0.98(-)}=-0.219\%$, $A_{amax}=0.120\%$ and $A_{a0.98(+)}=0.448\%$. Similar results, obtained for REBCO <100> with Cu are also shown in Fig. 5. In the whole region of strain measured, the values of I_{cr}/I_{c0} were always larger than 0.99 which again means that no degradation occurred. The maximum in critical current appeared at approximately zero applied strain. Again, the following parameters were obtained: $A_{a0.98(-)}=-0.300\%$, $A_{amax}=0.048\%$ and $A_{a0.98(+)}=0.360\%$.

Fig.6 shows the equivalent normalized critical currents, I_c/I_{c0} and I_{cr}/I_{c0} as a function of applied strain for REBCO <110> with Cu tape. Compared to the two previous cases of the <100> tapes in Fig. 5, the effect of the strain on both the normalized critical currents, I_c/I_{c0} and I_{cr}/I_{c0} is far smaller in the reversible compressive and tensile strain region. We also found that A_{a99} was 0.453 %, before the critical current decreased rapidly due to the brittle fracture of REBCO layer.

3.4 Change of local strain on REBCO layer

Synchrotron diffraction measurements were carried out to get direct information about the local strain exerted on the REBCO superconductive layer and investigate properly its effect on critical current. As shown in Fig. 7 for REBCO <100> with and without Cu, we paid particular attention to the diffraction peaks from the (200) and (020) crystal planes, where the scattering vector was kept along to the tape axis. Fig. 7 provides the diffraction data obtained under several different tensile strains, where the strain was increased by about 0.025 % in steps up to 0.7 %. As expected, the peak positions shifted towards larger lattice spacings with increasing strain.

The change of lattice spacing as a function of applied strain is indicated in Fig. 8 together with the stress-strain curve for both REBCO <100> with and without Cu tape. Their (200) and (020) lattice spacings increased linearly with increasing applied tensile strain up to about 0.5%. Here the solid straight line gives the following relation;

$$d(A) = d(0)[1 + \frac{A_a}{100}] \quad (1)$$

which suggests that the REBCO layer deforms elastically with increasing applied tensile strain. Beyond this linear part, a shoulder appeared in the stress-strain curve which we associate with prominent plastic deformation.

The data in Fig. 7 also show that the intensity profiles of both the (200) and (020) diffraction patterns overlap each other. By fitting a Gaussian curve to each diffraction peak, the observed intensity profiles were separated into two profiles and then their ratio (ϕ) were evaluated as follows,

$$\phi = \frac{\text{Integrated Intensity of (200) Diffraction}}{\text{Integrated Intensity of (020) Diffraction}} = \frac{f}{1-f} \quad (2)$$

Fig. 9 indicates the ratio (ϕ) of the integrated intensity of (200) diffraction to that of (020) for both REBCO <100> with and without Cu tape. The ratio remains in the range between 1.11 and 0.96 in the reversible strain region under about 0.5%. From the relation indicated in Eq. (2), the volume fraction f was estimated to be in the range between 0.526 and 0.490. The width of the peaks at their half intensity maximum was calculated from the two Gaussian curves and are shown in Fig. 10. The width for the (200) lattice spacing peak was broader than that of the (020) peak for both <100> tapes, with and without Cu tape.

In Fig. 11, the diffraction profiles observed for REBCO <110> with Cu tape are provided where the strain was increased in steps of about 0.025% up to 0.5 %. Because the <110> direction is parallel to the tape axis, a single diffraction peak for the (220) plane is recorded for the tapes under different tensile strains as shown in the figure. As expected, the peak position shifts towards larger lattice spacing. The change of lattice spacings as a function of applied strain is indicated in Fig. 12 together with the stress-strain curve for REBCO <110> with Cu tape. The lattice spacing increased linearly with increasing applied tensile strain up to about 0.5%. Here the solid straight line drawn along the linear part of observed lattice spacings is described by Eq. (1) which guarantees elastic tensile deformation without any local fracture.

In order to confirm the existence of the twinned structure for REBCO <110> with Cu tape, the diffraction pattern was measured after the tape was rotated by 45 degrees from the scattering vector axis. As shown in Fig. 13, the double peak behavior due to (200) and (020) lattice planes was observed. From Eq. (2), the factor f was evaluated as 0.52.

4. Discussion and Analysis

4.1 One-dimensional twin model for REBCO tapes

The two types of REBCO composite tapes investigated here have their crystal orientation along the tape axis which is in one case parallel to $\langle 100 \rangle$ and in the other parallel to $\langle 110 \rangle$ as shown in Fig. 14. As shown in Fig. 14 (a), the A[100]- and B[010]-domains continue repeatedly along the uniaxial strain direction for the $\langle 100 \rangle$ oriented tape. On the other hand, both a - and b -axes are inclined at 45 degrees from the tape axis for the $\langle 110 \rangle$ oriented tape as shown in Fig. 14 (b). The different orientation of twin structure along the tape axis results in the different strain dependencies for the critical current as discussed below.

4.2 Strain dependence of critical current for the $\langle 100 \rangle$ oriented tape

Fig. 14(a) provides an important elementary unit of the $\langle 100 \rangle$ oriented structure, where the current flows cross repeatedly over both A[100]- and B[010]- domains. Following Ref. [20], we can expect the strain dependence of I_c to be different in the two domains. In each region of Fig. 14(a), the local electric-field – current (E - I) characteristics of a high current superconductor are empirically described by,

$$E = E_C \left(\frac{I}{I_{C,hkl}} \right)^n \quad (3)$$

where E_C is the electric field at which the critical current I_c is defined and n is known as the index of transition. Following the considerations given in the Annex, the critical current in the A[100]- and the B[010]- domains can be described using;

$$I_{C,100} = I_C(0)[1 + g_{100}A_a] \quad (4)$$

$$I_{C,010} = I_C(0)[1 + g_{010}A_a] \quad (5)$$

where A_a is the applied strain and g_{100} and g_{010} are proportionality constants. Given the critical current I_c is defined when the electric field E_c becomes $1 \mu\text{V}/\text{cm}$, the electric field E_c is given by the equation,

$$E_C = fE_{100} + (1 - f)E_{010} \quad (6)$$

By using Eqs. 3 – 6, the following relationship is derived,

$$1 = f \left\{ \frac{I_c}{I_C(0)(1+g_{100}A_a)} \right\}^n + (1 - f) \left\{ \frac{I_c}{I_C(0)(1+g_{010}A_a)} \right\}^n \quad (7)$$

As shown in Fig. 14(a), there are A[100]-domains and B[010]-ones oriented along the uniaxial strain direction [25] with fractional length of the two domains given by f and $(1 - f)$, respectively. Within the A[100]-domain, the unit cell has the a-lattice parameter parallel to the uniaxial strain which means the Cu-O chains are orthogonal to the uniaxial strain. Within the B[010]-domain, the Cu-O chains are parallel to the uniaxial strain axis and to the current flow direction. So for the $\langle 100 \rangle$ tape, we can take as

$$g_{100} = -g_{010} \equiv g_0 \quad (8)$$

In this case, the critical current I_c is as reported in Ref [20] and given by,

$$I_c = I_c(0)\{1 - (1 - 2f)g_0A_a - 2(1 - f)f(1 + n)g_0^2A_a^2 + O[A_a^3]\} \quad (9)$$

Eq. (9) is plotted as a function of applied strain g_0A_a in Fig. 15. The most important features are the inverted parabolic strain behavior for the critical current and that the maximum position shifts towards the tensile strain side when the volume fraction f is larger than 0.5 and vice versa. Also as mentioned previously [20], a thermal residual strain generates in the SC layer during cooling, which can also influence the maximum position of critical current. The inverted parabolic strain behavior predicted by Eq. (9) is clearly shown in the experimental data in Fig. 5 for the $\langle 100 \rangle$ oriented tapes.

4.3 Strain dependence of critical current for the $\langle 110 \rangle$ oriented tape

Fig. 14(b) provides the domain structure of the $\langle 110 \rangle$ oriented tape along the uniaxial load direction. The a and b axes are inclined by 45 degrees to the current flow direction in both the A- and B- domains which means the strain affects both domains in the same way. When applying the external strain along the [100] or [010] direction, the strain produces a change of lattice constant $\Delta a/a$ in the a-direction and $\Delta b/b$ in the b-direction as shown in Fig. 16. Hence the lattice parameter change along [110] can be approximated by $(\Delta a + \Delta b)/(a^2 + b^2)^{1/2}$. In Eq. (8), instead of two terms, g_{100} and g_{010} , as required for the $\langle 100 \rangle$ tape, a single g_{110} term is required since both domains respond in a similar way and the following relation is obtained,

$$I_c = I_c(0)[1 + g_{110}A_a] \quad (10)$$

Unfortunately to our knowledge, there are no detailed measurements on REBCO single-crystals of the effect of strain on T_c as a function of angle in the a - b plane. Hence we assume that the parameter $g(\theta)$ in each domain can simply be approximated as [26] ;

$$g(\theta) = g_{100} \cdot \cos(\theta) + g_{010} \cdot \sin(\theta) \quad (11)$$

where θ is the angle between the direction of the applied strain and the a -axis. Eq. (11) is consistent with the limited experimental results on REBCO single crystals that show a tensile strain in the a -direction increases the critical temperature T_c whereas a tensile strain in the b -direction decreases T_c . Eq (11) is consistent with angular averaging in a single domain for example if we apply a strain with tensile components in both a - and b -directions. It is also consistent with recent work showing that both a weak, and an inverted parabolic strain behavior, can both be found experimentally in a single $\langle 100 \rangle$ tape if the strain is applied at 45 degrees to the axis of the tape, and along the tape respectively [26]. For the $\langle 110 \rangle$ tapes investigated here, we use Eq. (8) and find for the special case when $\theta = 45^\circ$, Eq. (11) leads to :

$$g_{110} = g_{100} \cdot \cos(45^\circ) + g_{010} \cdot \sin(45^\circ) = 0 \quad (12)$$

Hence the resultant external strain dependence of I_c for the $\langle 110 \rangle$ tape is given by Eq. (10) where we expect g_{110} to be small - indeed zero when Eq (8) holds. For the $\langle 110 \rangle$ tapes, as required, Eq (10) also has no f - dependence since as can be seen in Fig. 14, when the direction the strain is applied is at 45 degrees to both the a - and b -axes, the relative proportions of the two possible domains does not change the overall strain-dependence of the tape. We conclude that Eqs. (10) and (12) provide a straightforward explanation for the weak uniaxial strain dependence for the $\langle 110 \rangle$ oriented tape shown in Fig. 6.

5. Conclusion

In the present study, two types of practical REBCO tape have been examined, in which the crystal orientation along the tape axis is parallel to $\langle 100 \rangle$ or $\langle 110 \rangle$. We have used two different I_c measurement techniques and investigated their uniaxial strain dependence of critical current. One of the techniques had the sample attached directly to the universal testing machine and was pulled by a tensile load. The other used a springboard on which the sample is soldered, was attached the testing machine and then was pushed or pulled in order to apply both tensile and compressive strains to the tape sample. An inverted parabolic behavior was observed in the uniaxial strain dependence for the critical current for the $\langle 100 \rangle$ oriented tapes. In contrast, the $\langle 110 \rangle$ oriented REBCO tape does not give any maximum on its strain dependence. We have also reported using synchrotron radiation diffraction to measure the local strain exerted on the REBCO layer at room temperature using the same two techniques for straining the tape as for I_c

measurements. On the basis of the observed data, the local strain exerted on the REBCO layer at 77 K was evaluated and the elastic regime clearly identified.

The focus for the present study is to explain why the strain dependence of critical current behaves for the <100> and <110> oriented REBCO tapes are different. The results for the <100> and <110> oriented REBCO tapes have been compared using a common structure model, which is one-dimensional twin (or chain) model for REBCO material with fractional lengths of A-domains and B-domains. It has been made clear that the present approach can reproduce all the broad features of the experimental results on both tapes for the uniaxial strain dependence of the critical current.

Acknowledgements:

This work was supported in part by a grant-in-aid of the Ministry of Education, Culture, Sports, Science and Technology, Japan (26420669). The synchrotron radiation experiments were performed at the BL28B2 of SPring-8 with the approval of the Japan Synchrotron Radiation Research Institute (JASRI) (Proposal No. 2017A1108). This work was funded by EPSRC under grant EP/K504178/1. The data in this paper and associated materials are on the Durham Research Online website: <http://dro.dur.ac.uk/>. We acknowledge useful discussions with J Greenwood.

Appendix:

According to the study [27] on the strain-controlled critical temperature in REBa₂Cu₃O_y-coated conductors, it was reported that the critical temperature increases with increasing strain along the [100] direction, but it decreases with increasing strain along the [010] one. Their strain dependence can be expressed in the linear form in the small external strain region as follows;

$$T_{C,100} = T_C(0)[1 + q_{100}^* A_a] \quad (\text{A1})$$

$$T_{C,010} = T_C(0)[1 + q_{010}^* A_a] \quad (\text{A2})$$

where A_a [%] is the externally applied strain. By using the original data reported in [25], the parameters were evaluated as $q_{100}^* = 0.042 \sim 0.046$ and $q_{010}^* = -0.046 \sim -0.042$. So, in order to keep algebra straightforward in our present discussion, we put for the <100> tape that $q_0 = q_{100}^* = -q_{010}^*$. According to the Ekin's scaling law [16], the magnitude of critical current is related with the critical temperature via the relationship with the upper critical field. Thus, the strain dependence of critical current given by Eqs. (4) and (5) in the main text is assumed to keep the similar dependence with Eqs. (A1) and (A2).

References

- [1] IEC 61788-20:2014 Superconductivity- Superconducting wires - Categories of practical superconducting wires - General characteristics and guidance
- [2] K Osamura, S Machiya, Y Tsuchiya, H Suzuki, 2010 Force free strain exerted on a YBCO layer at 77 K in surround Cu stabilized YBCO coated conductors, Supercond. Sci. Technol. **23** 045020-045026
- [3] K Vinod, R G Abhilash Kumar and U Syamaprasad 2007 Prospects for MgB₂ superconductors for magnet application. Supercond. Sci. Technol. **20** R1-R13.
- [4] K Osamura, S Machiya, H Suzuki, S Ochiai, H Adachi, N Ayai, K Hayashi and K Sato, 2008 Mechanical Behavior and Strain Dependence of the Critical Current of DI-BSCCO Tapes, Supercond. Sci. Technol. **21** 054010-054018.
- [5] S Ochiai and H Okuda, 2011 Residual Strain. Damage Strain and Critical Current in BSCCO Tape, J. Cryo. Soc. Jpn., **46** 212-219
- [6] K Osamura, S Machiya, Y Tsuchiya, H Suzuki, T Shobu, M Sato and S Ochiai, 2012 Microtwin Structure and Its Influence on the Mechanical Properties of REBCO Coated Conductors, IEEE Transactions on Applied Superconductivity, **22** 8400809(9pp)
- [7] K Ilin, K A Yagotintsev et al, 2015 Experiments and FE Modeling of Stress – Strain State in ReBCO Tape under Tensile, Torsion and Transverse Load, Supercond. Sci. Technol. **28** 055006 (17 pp)
- [8] T Suzuki, S Awaji, H Oguro and K Watanabe, 2015 Applied strain effect on superconducting properties for detwinned (Y,Gd)BCO coated conductor”, IEEE Trans. Applied Superconductivity, **25** , 8400704
- [9] K Osamura, S Machiya, Y Tsuchiya, H Suzuki, T Shobu, M Sato, S Harjo, K Miyashita, Y Wadayama, S Ochiai and A Nishimura, 2013 Thermal Strain Exerted on Superconductive Filaments in Practical Nb₃Sn and Nb₃Al Strands, Supercond. Sci. Technol. **26** 094001 (8pp).
- [10] H Oguro, S Awaji, K Watanabe, M Sugano, S Machiya, T Shobu, M Sato, T Koganezawa and K Osamura, 2012 Internal strain measurement for Nb₃Sn wires using synchrotron radiation, Supercond. Sci. Technol., **25** 054004(4pp)
- [11] D Arbelaez, A Godeke and S O Prestemon, 2009 An improved model for the strain dependence of the superconducting properties of Nb₃Sn, Supercond. Sci. Technol. **22** 025005 (6pp).
- [12] D M J Taylor and D P Hampshire, 2005 The scaling law for the strain dependence of the critical current density in Nb₃Sn superconducting wires, Supercond. Sci. Technol. **18** S241–52
- [13] D S Easton and R E Schwall, 1976 Performance of Multifilamentary Nb₃Sn under Mechanical Load, Apply. Phys. Letter. **29** 319.

- [14] N Cheggour, A Nijhuis, H J G Krooshoop, X F Lu, J Splett, T C Stauffer, L F Goodrich, M C Jewell, A Devred, and Y Nabara, 2012 Strain and Magnetic-Field Characterization of a Bronze-Route Nb₃Sn ITER Wire: Benchmarking of Strain Measurement Facilities at NIST and University of Twente, *IEEE Trans. Appl. Supercond.* **22** 4805104.
- [15] K Osamura, S Machiya, S Harjo, T Nakamoto, N Cheggour and A Nijhuis, 2015 Local Strain Exerted on Nb₃Sn Filaments in an ITER Strand, *Supercond. Sci. Technol.* **28** 045016 (9pp)
- [16] J W Ekin, 1980 Strain scaling law for the flux pinning in practical superconductors. Part 1: basic relationship and application to Nb₃Sn conductor, *Cryogenics* **20** 611
- [17] K Osamura, S Machiya, D P Hampshire, Y Tsuchiya, T Shobu, K Kajiwara, G Osabe, K Yamazaki, Y Yamada and J Fujikami, 2014 Uniaxial strain dependence of the critical current of DI-BSCCO tapes *Supercond. Sci. Technol.* **27** 085005 (11pp)
- [18] C Senatore, C Barth, M Bonura, M Kulich and G Mondonico, 2016 Field and Temperature Scaling of the Critical Current Density in Commercial REBCO Coated Conductors, *Supercond. Sci. Technol.*, **29** 014002 (8 pp)
- [19] K Osamura, S Machiya, Y Tsuchiya, H Suzuki, 2010 Internal Strain and Mechanical Properties at Low Temperatures of Surround Cu Stabilized YBCO Coated Conductor, *IEEE Transaction on Applied Superconductivity*, **20** 1532-1536
- [20] K Osamura, S Machiya and D Hampshire, 2016 Mechanism for the uniaxial strain dependence of the critical current in practical REBCO tapes, *Supercond. Sci. Technol.* **29** 065019 (17pp)
- [21] P Sunwong, J S Higgins and D P Hampshire, 2011 Angular, temperature and strain dependencies of the critical current of DI-BSCCO tapes in high magnetic fields, *IEEE Trans. Appl. Supercond.* **21** 2840–4
- [22] <http://www.superpower-inc.com/content/2g-hts-wire>
- [23] <http://www.fujikura.com/solutions/superconductingwire/>
- [24] IEC 61788-25:2018 Superconductivity – Superconducting wires - Mechanical properties measurement – Room temperature tensile test on REBCO wires
- [25] D M J Taylor and D P Hampshire, 2015 Properties of helical springs used to measure the axial strain dependence of the critical current density in superconducting wire, *Supercond. Sci. Technol.* **18**, 356-368
- [26] The Biaxial Strain Dependence of J_C of a (RE)BCO Coated Conductor at 77 K in Low Fields. Jack R. Greenwood, Elizabeth Surrey and Damian P. Hampshire submitted to *IEEE Trans. Appl. Super. Oct.* 2018.
- [27] S Awaji, *et al.*, 2015 Strain-controlled critical temperature in REBa₂Cu₃O_y-coated conductors. *Sci. Rep.* **5**, 11156

Tables

Table 1 Characteristic dimension of the components of REBCO tapes investigated in the present project

Sample Name	REBCO <100> without Cu	REBCO <100> with Cu	REBCO <110> with Cu
Tape thickness (mm)	0.054	0.070	0.22
Tape width (mm)	4.0	2.0	5.0
Thickness of Hastelloy substrate (micron)	50	50	100
Thickness of Cu lamination (micron)	no	15	100
REBCO thickness (micron)	1.65	1.65	1.1
Rare earth element of REBCO layer	Y _{0.5} Gd _{0.5}	Y _{0.5} Gd _{0.5}	Gd

Table 2 Summary of mechanical properties for three REBCO tapes

Sample Name	Temperature	E_U (GPa)	$R_{0.2}$ (MPa)	$A_{0.2}$ (%)
REBCO <100> without Cu	RT	185	1021	0.748
	77K	194	1270	0.855
REBCO <100> with Cu	RT	166	876	0.738
	77K	168	1076	0.857
REBCO <110> with Cu	RT	141	744	0.716
	77K	168	960.5	0.755

Table 3 Summary of 99% recovery and 95% retention

Sample Name	99% Recovery		95% Retention	
	A_{99} (%)	R_{99} (MPa)	A_{95} (%)	R_{95} (MPa)
REBCO <100> without Cu	0.385	760	0.377	750
REBCO <100> with Cu	0.453	739	0.400	653
REBCO <110> with Cu	0.455	642	0.461	654

Table 4 Summary of characteristic strain parameters for the <100> oriented tapes

	$A_{a0.98(-)}$ (%)	A_{amax} (%)	$A_{a0.98(+)}$ (%)	$ A_{a0.98(-)}-A_{amax} $ (%)	$ A_{a0.98(+)}-A_{amax} $ (%)
<100> without Cu	-0.219	0.120	0.448	0.339	0.328
<100> with Cu	-0.300	0.048	0.360	0.348	0.312

Figures

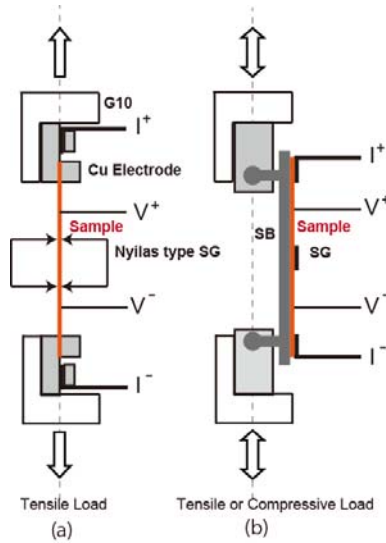


Fig. 1 Two techniques for evaluating the uniaxial strain dependence of I_c , where G10 is an insulator, SG is a strain gauge, and SB is the springboard.

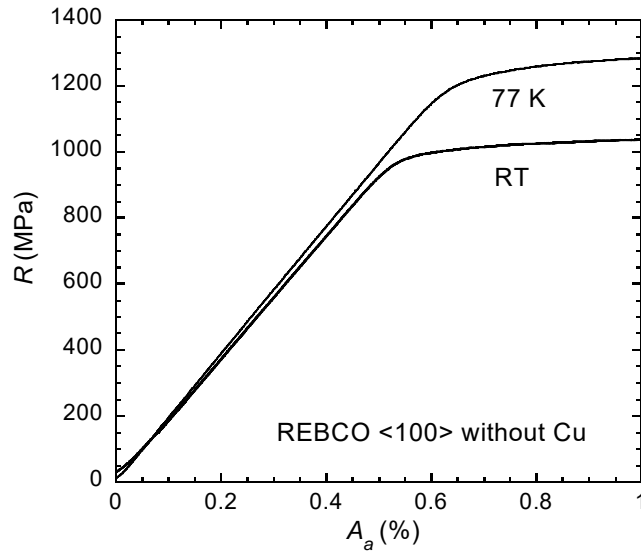


Fig.2 Stress – strain curve at RT and 77 K for REBCO <100> without Cu tape

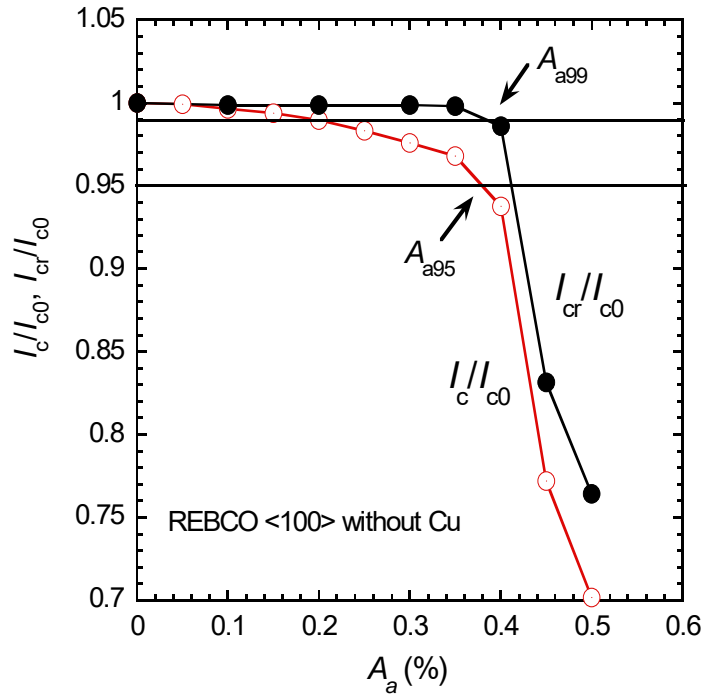


Fig. 3 Applied strain dependence of normalized critical currents, I_c/I_{c0} and I_{cr}/I_{c0} for REBCO <100> without Cu tape

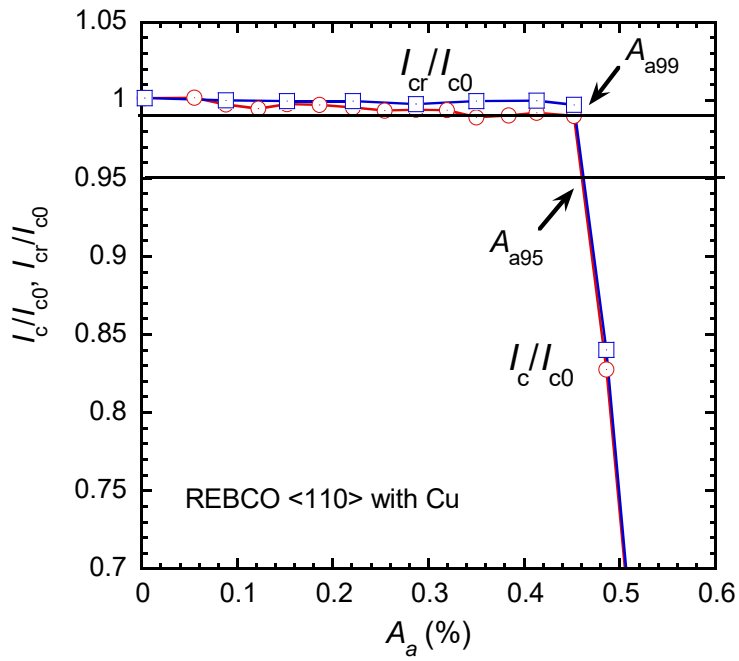
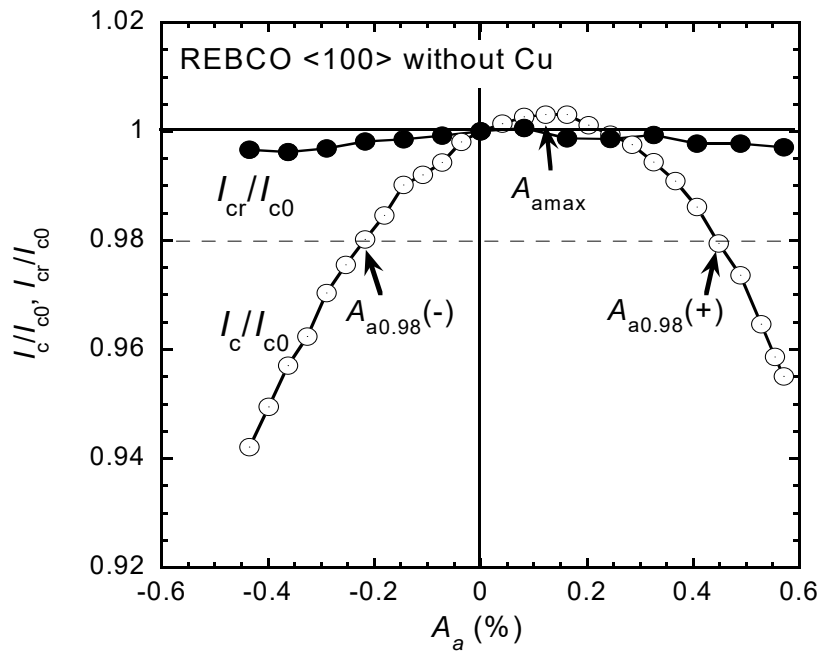
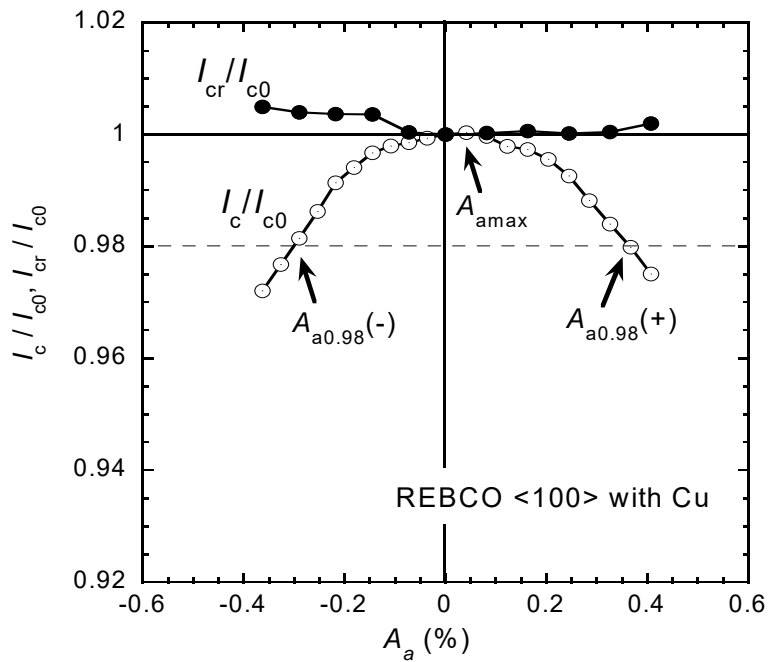


Fig. 4 Applied strain dependence of normalized critical currents, I_c/I_{c0} and I_{cr}/I_{c0} for REBCO <110> with Cu Tape



(a)



(b)

Fig. 5 Uniaxial strain dependence of the normalized critical current for (a) REBCO <100> without Cu tape and (b) REBCO <100> with Cu tape.

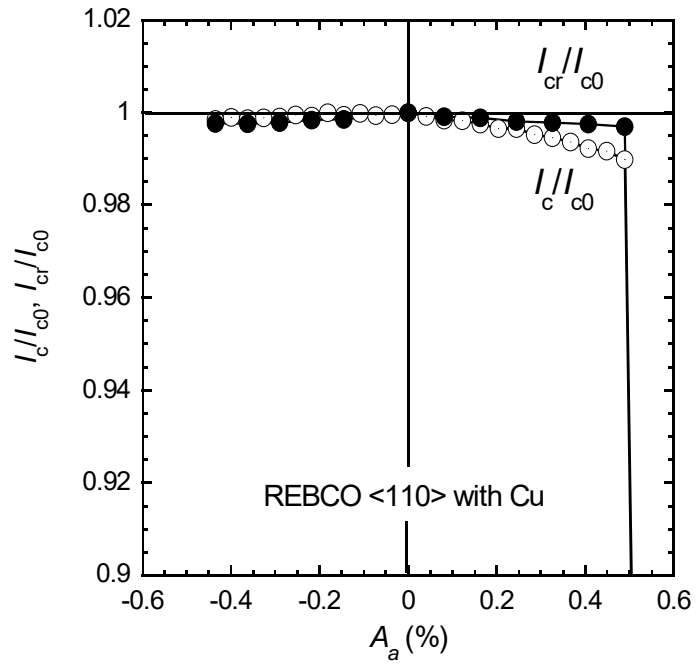
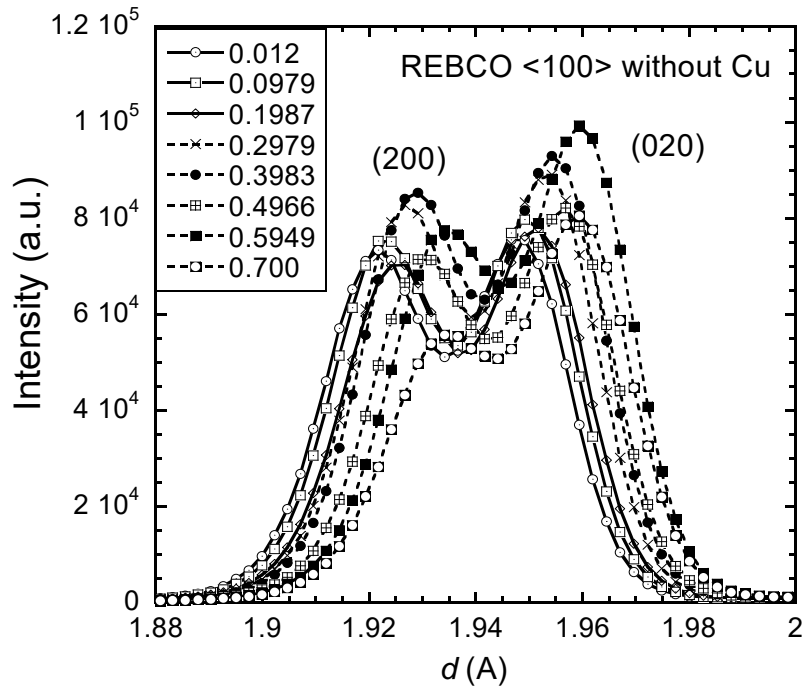
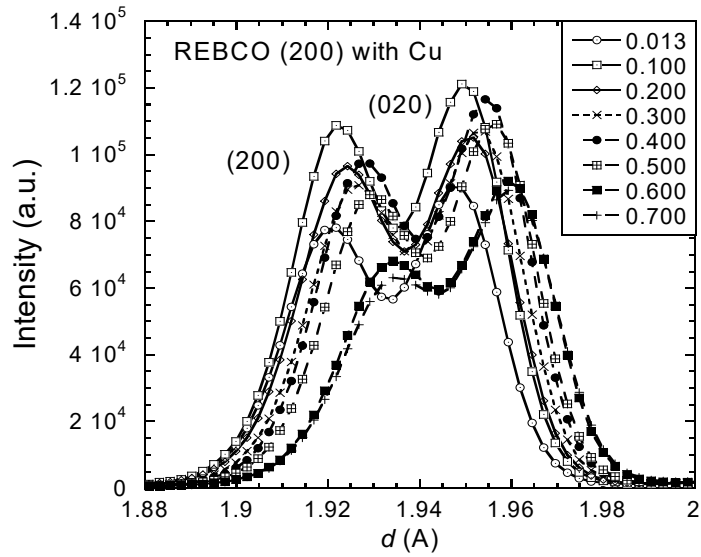


Fig. 6 Uniaxial strain dependence of the normalized critical current for REBCO <110> with Cu tape

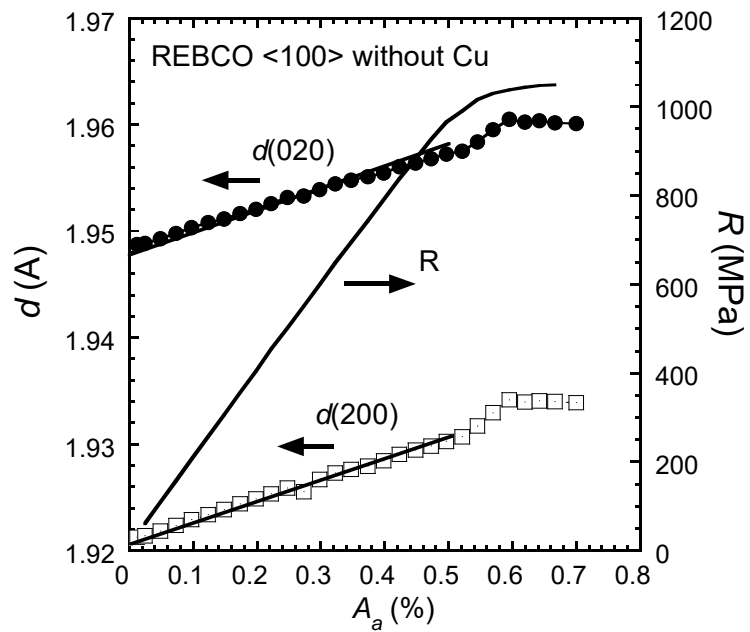


(a)

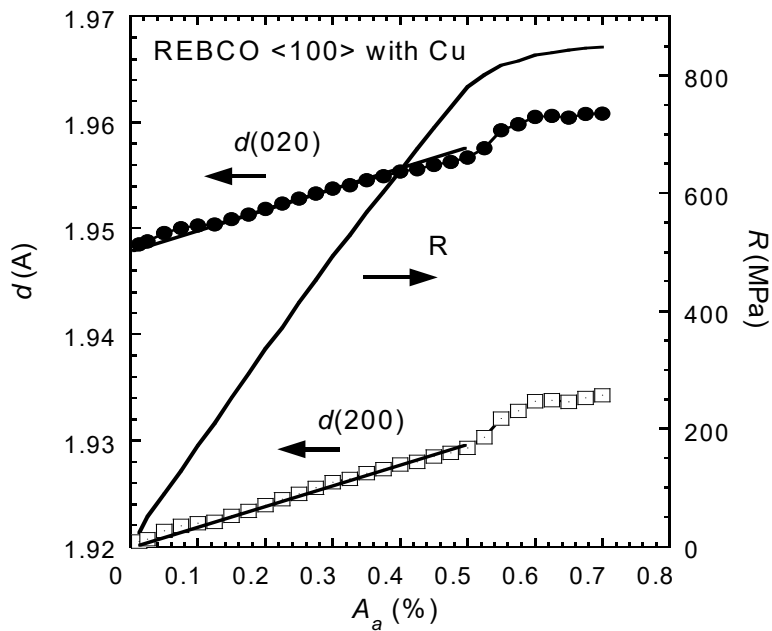


(b)

Fig. 7 Typical diffraction profiles of the (200) and (020) planes of the $\text{REBa}_2\text{Cu}_3\text{O}_{8+x}$ phase while increasing the applied tensile strain as indicated in the figure. (a): for REBCO <100> without Cu tape. (b): for REBCO <100> with Cu tape



(a)



(b)

Fig. 8 Applied tensile strain dependence of lattice spacing $d(200)$ and $d(020)$ together with the stress – strain curve. (a): for REBCO <100> without Cu tape. (b): for REBCO <100> with Cu tape

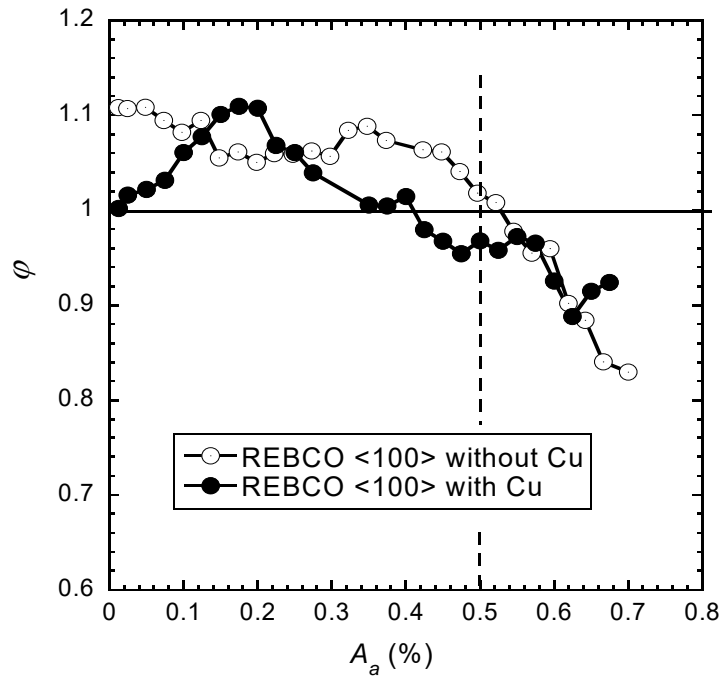


Fig. 9 Tensile strain dependence of the ratio (ϕ) of the integrated intensity of (200) diffraction to that of (020) one for both REBCO <100> with and without Cu tape

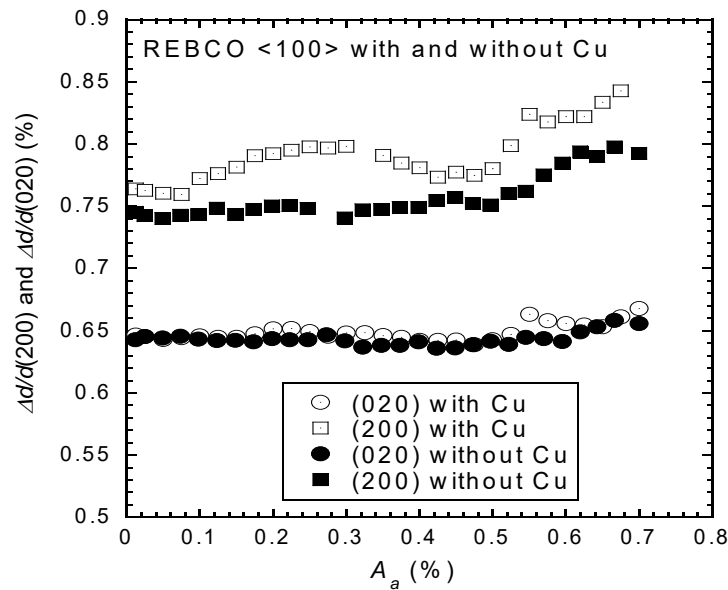


Fig. 10 Width at half maximum intensity divided by the peak (200) and (020) lattice spacings, as a function of applied strain for the REBCO <100> tapes with and without Cu.

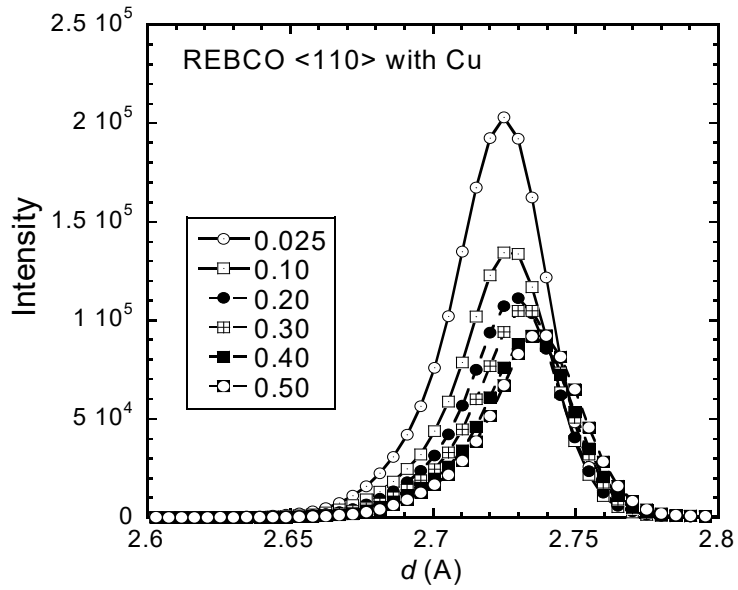


Fig.11 Diffraction profiles due to (220) plane of $\text{REBa}_2\text{Cu}_3\text{O}_{8+x}$ phase during the increase of applied tensile strain for REBCO <110> with Cu tape

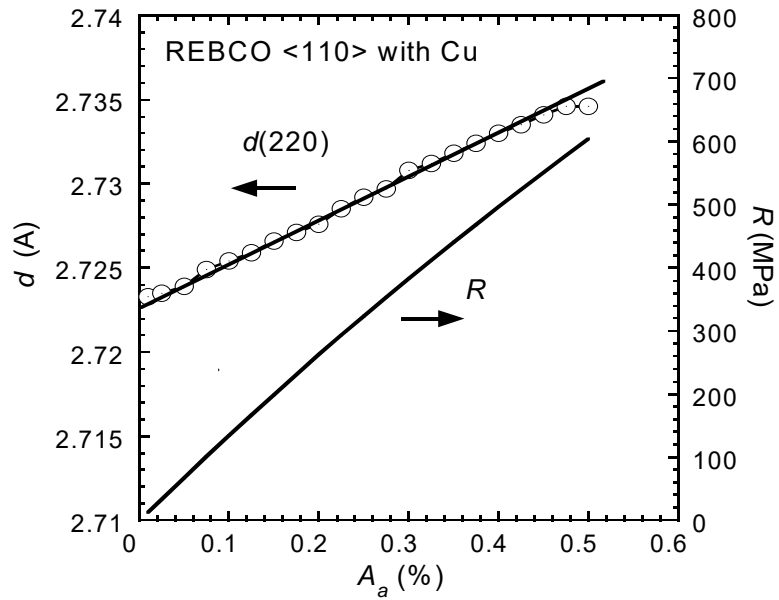


Fig.12 Applied tensile strain dependence of lattice spacing $d(220)$ together with the stress – strain curve for REBCO <110> with Cu tape

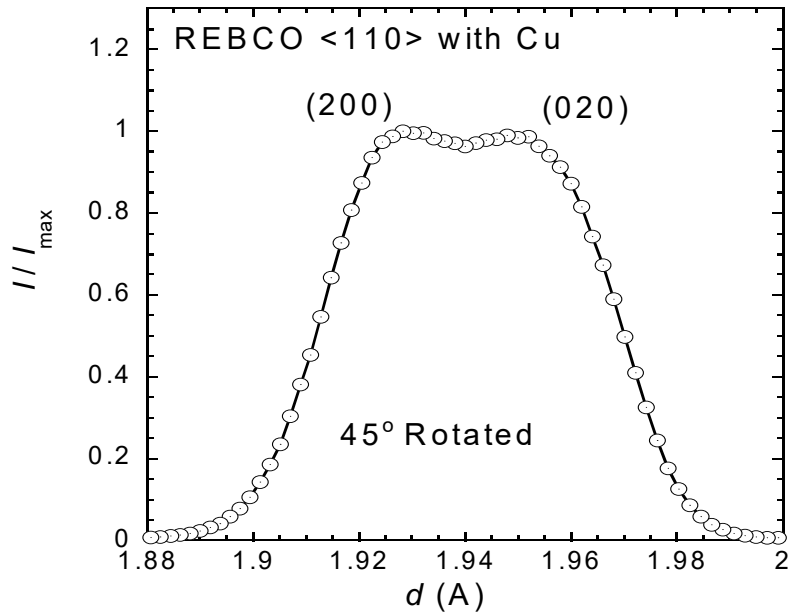


Fig. 13 Diffraction pattern of (200) and (020) lattice planes at the 45 degrees rotated position from the scattering vector axis for REBCO <110> with Cu tape

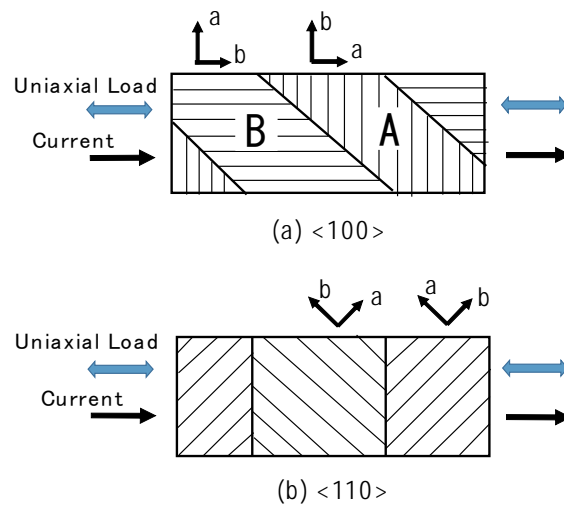


Fig. 14 <100> and <110> oriented twin structures along the tape axis

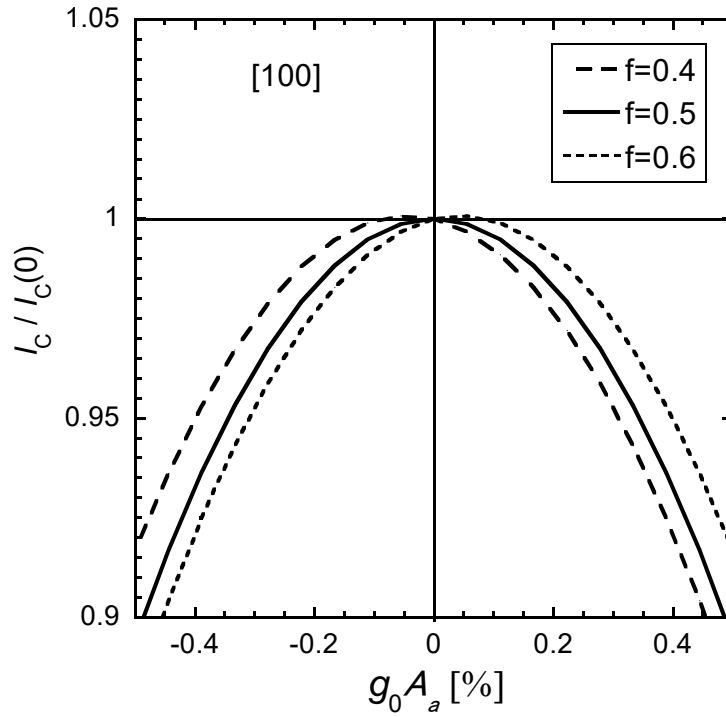


Fig. 15 The normalized critical current as a function of $g_0 A_a$ for the $\langle 100 \rangle$ oriented tape with different volume ratio of A- and B- domains.

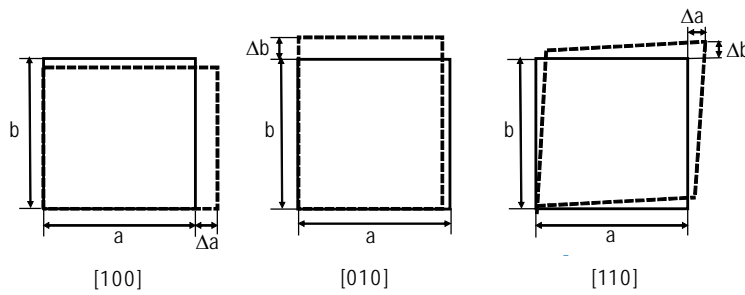


Fig. 16 A principal lattice change by one dimensional deformation along various crystal orientations.